Elucidating Electrocatalytic Oxygen Reduction Kinetics via Intermediates by Time Resolved Electrochemiluminescence

Kaiqing Wu, Ran Chen, Zhixin Zhou, Xinghua Chen, Yanqin Lv, Jin Ma, Yanfei Shen, Songqin Liu, Yuanjian Zhang*

Jiangsu Engineering Laboratory of Smart Carbon-Rich Materials and Device, Jiangsu Province Hi-Tech Key Laboratory for Bio-Medical Research, State Key Laboratory of Bioelectronics, School of Chemistry and Chemical Engineering, Medical School, Southeast University, Nanjing 21189, China. Email: Yuanjian.Zhang@seu.edu.cn

Abstract

Rapid and accurate evaluation of oxygen reduction reaction (ORR) kinetics for massive potential electrocatalysts is critical for developing sustainable energy conversion devices. In principle, both the consumption rate of O_2 and production rate of reactive oxygen species (ROS) intermediates can be used to establish the ORR rate equation. Notably, owing to the grand challenge in quantitative *in-situ* detection of trace-amount of ROS, most previous ORR kinetics studies rely on direct electrochemical examination of O_2 consumption, but which is inevitably hampered by the slow mass transfer of O_2 in electrolytes. Here we report a time resolved electrochemiluminescence (Tr-ECL) strategy to establish ORR rate equation via ultra-sensitive detection of ROS intermediates. As ROS were generated at electrocatalysts surfaces in the diffusion layer, it intrinsically circumvented the limit of mass transfer of O_2 in electrolytes during ORR. As a result, ORR electron transfer numbers, rate constants, and ROS concentration-potential correlations that is closely related to the stability of electrocatalysts were successfully obtained by principal component analysis of ECL intensities and finite elemental analysis of time-resolved ECL decay curves. It provides a rapidly, precisely, and facile way to understand ORR mechanism and would greatly pave development of electrocatalysts with appropriate catalytic activity, selectivity and stability.

Keywords: Oxygen reduction reaction, Kinetics, Electrocatalysts, Reactive oxygen species, Time resolved electrochemiluminescence

Introduction

Carbon neutrality is widely regarded as the ultimate way to address global warming and achieve a sustainable world. Among them, fuel cells have garnered increasing attention as a promising solution since it does not emit carbon dioxide during the conversion of chemical energy into electricity and the theoretical efficiency is near-unity.[1-6] However, owing to multiple electron-transfer processes, the oxygen reduction reaction (ORR, Figure 1), the cathodic reaction in fuel cells, is kinetically sluggish, which greatly hampered the commercialization of fuel cells.[7] Along this line, developing ORR electrocatalysts with high activity, reasonable durability and low cost has been intensively explored for several decades.[8-10] To accelerate research and development, accurate and fast screening ORR activity of massive electrocatalyst candidates is highly envisioned, but still remain challenges.

The membrane electrode assembly (MEA), primarily consisting of the proton exchange membrane, catalyst layer and gas diffusion layer, is the closest to the real fuel cell use.[2, 11] Nevertheless, its operation is time-consuming and need costly equipment, professional expertise, and large quantity of samples.[12] In this event, newly developed electrocatalysts which is often in small amounts are preferred to be examined by laboratory testing, prior to apply in MEA or realistic fuel cells. For this reason, the rotation electrode technique, including rotating disk electrode (RDE) and rotating ring disk electrode (RRDE), has been the most common way to obtain the intrinsic activities of ORR catalysts.[13-16] The Koutecky-Levich (K-L) equation describes current density of electrocatalysts on RDE (Eq. S1-3). The selectivity of H_2O_2 and the associated electron transfer number (n) during ORR can also be calculated by RRDE (Eq. S4, 5). However, electrocatalysts with high activities exclusively obtained from RDE and RRDE measurements have rarely translated into practical fuel cell performance due to the low mass-transfer resistance of oxygen in the aqueous electrolytes, although a forced convection by rotation of electrode over thousands rounds per minute has been already applied.[16] To further improve current density approaching MEA, floating electrode technique (FET) with a porous diffusion electrode at gas/aqueous electrolyte interface was proposed with great success; the future improvements include precise

pressure and flow rate control, reproducibility, and standardization.[17-18] Alternatively, thanks to ultramicroelectrodes (UME) giving hemispherical diffusion, scanning electrochemical microscopy (SECM) provides another intriguing way to achieve useful steady-state conditions, but the scanning area and probe types require specialized topography of electrocatalysts, restricting its broad application.[19-22]

Despite unprecedented advances, notably, few of them use the reactive oxygen species (ROS) intermediates to establish reaction rate equations.[22-24] Indeed, ROS are produced in the diffusion layer at a much lower concentration than O_2 and of short life, making the mass diffusion resistance in the bulk solution negligible. Thus, we hypothesize that if the reaction rate equation was established using the ROS intermediate instead of O_2 in previous methods, the long-term concern of mass transport limitation for O_2 would be avoided in principle. Moreover, the generation of ROS is an indispensable step in ORR, and, are supposed to be closely correlated to the degradation of electrocatalyst in operating. However, facile quantification of ROS intermediates of trace-amount and short life in ORR are generally challenging.

Due to theoretical zero background and simple instrumentation, electrogenerated chemiluminescence (ECL) has drawn increasing attention across diverse fields, ranging from clinical diagnosis to super-resolved imaging.[25-30] As known, ROS are excellent co-reactants for luminol to gain strong ECL signal.[31-32] For instance, the detection limit of H_2O_2 by ECL via $O_2^{\bullet-}$ pathway (Eq. S9-16) was three orders of magnitude superior to that by RRDE (Figure S1). Thus, ROS-triggered ECL would be a facile and highly sensitive tool to screen kinetics of ORR electrocatalysts; however, except for few works on ECL-imaging of single particles qualitatively acquiring active site distribution, it has been rarely explored.[33]

Herein, we report a ROS-oriented strategy for kinetic evaluation of ORR electrocatalysts using ultrasensitive time resolved ECL (Tr-ECL) in a conventional three-electrode electrochemical cell configuration. It consisted of synchronous ECL intensity collection and sequential ORR/ECL reactions driven by double-potential step chronoamperometry. Only commonly-used glassy carbon working electrodes in a stationary condition is needed to detect trace-amount of ROS intermediates in the

diffusion layer, which greatly simplified the instrumentation with respect to RDE/RRDE, FET, SECM and MEA. As a result, variable electrocatalysts with two-/four-electron reduction could be rapidly discriminated by principal component analysis (PCA). Moreover, by finite element analysis (FEA) of the ECL decay curves, the quantitative kinetic information, such as apparent rate constant and the dependence of ROS concentration/distribution at different potentials that is closely related to the stability of electrocatalysts were successfully extracted. The proposed Tr-ECL method provides a rapidly, precisely, and facile way to understand ORR mechanism and pave development of electrocatalysts with appropriate catalytic activity, selectivity and stability.

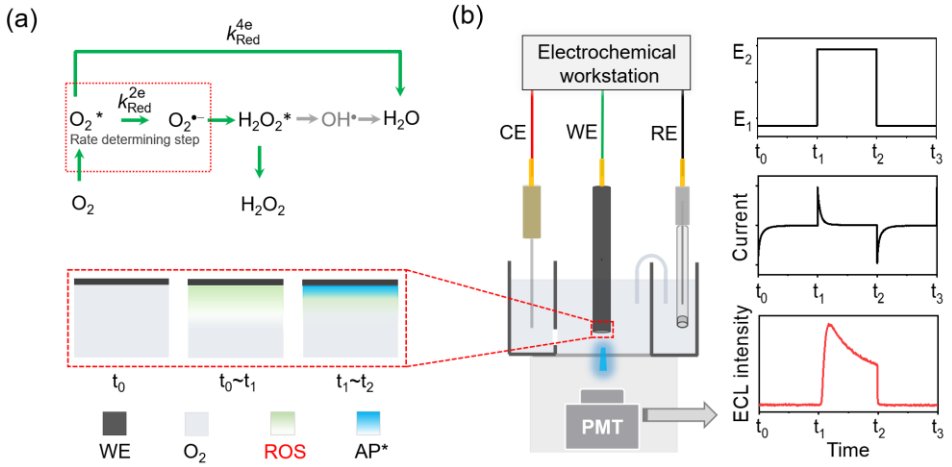

Figure 1. (a) Reaction pathways of ORR in a modified Damjanovic model; (b) Brief setup of Tr-ECL methods for ORR kinetics analysis. The enlarged area and line charts show the distribution of dissolved O_2, ROS, and Ap* in the diffusion layer and the electrochemical/ECL signals at different time during the Tr-ECL measurement.

Results and discussion

The widely accepted Damjanovic model with modification for the ORR is shown in Figure 1a. [34-35] In general, it consists of several parallel steps. In the typical four-electron ($4e^-$) transfer pathway, O_2 is directly reduced into H_2O by accepting four electrons. Sequential pathway involving two-electron ($2e^-$) reduction of O_2 to H_2O_2 and a further reduction by another $2e^-$ reduction to water is also proposed in previous reports. Alternatively, the reaction is stopped at the generation of H_2O_2, which is the

representative $2e^-$ transfer pathway. For most electrocatalysts, $2e^-$ and $4e^-$ transfer pathways parallelly occur. Along the line, there were four preconditions for ECL to be applicable in ORR kinetics evaluation: (1) whether ROS were generated in ORR; (2) would ROS trigger chemiluminescence of luminol; (3) could short-lived ROS produced during ORR be stable until the chemiluminescence was triggered; and (4) the influence of exotic luminol on ORR is negligible or not.

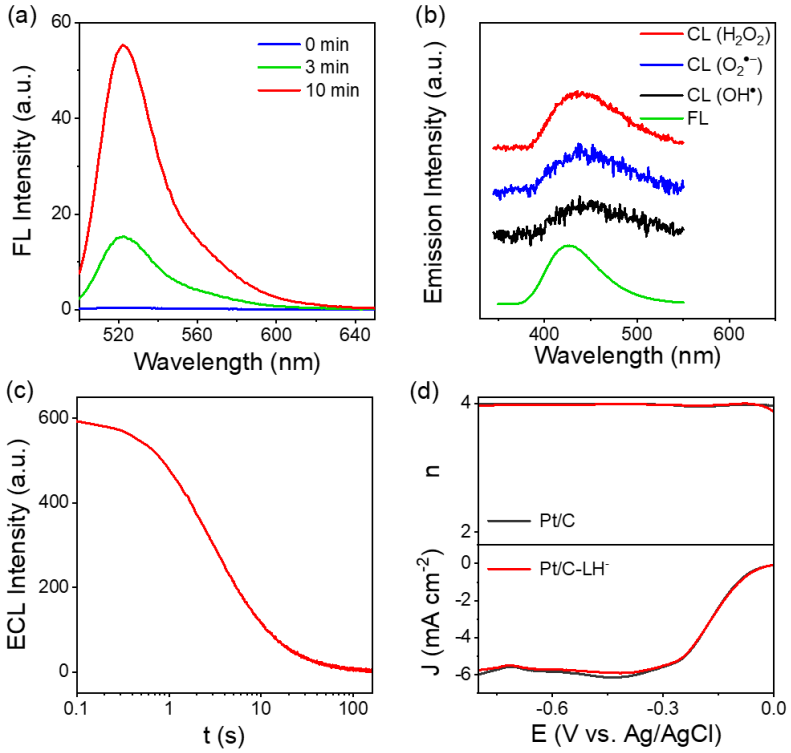

Figure 2. Principle verification of ECL for ORR kinetics evaluation. (a) Fluorescence spectra of DCDFH after reaction with ROS generated by ORR with different accumulated time. (b) Chemiluminescent (CL) spectra of luminol in presence of H_2O_2 (red line), $O_2^{\bullet-}$ (blue line), $OH^{\bullet}$ (black line) and FL spectrum of luminol (green line). (c) Intensity of ROS triggered ECL with time when ORR was off. (d) Electron transfer number (n) and polarization curves for Pt/C by RRDE in O_2-saturated 0.1 M KOH with and without luminol.

To validate these requirements, in the first set of experiments, 2,7-dichlorodihydrofluorescein diacetate (DCDFH) was used as an intermediate indicator, as it can chemically react with ROS forming a fluorescent product.[36] Taking Zn-N-C for example, it was observed that the typical fluorescence for oxidized product of DCDFH appeared when a potential of -0.3 V was applied to drive ORR, and the fluorescent intensity accumulated upon the extended reaction time (Figure 2a, Figure

S2). It evidently verified the production of ROS in ORR. Complementarily, the trapping experiments for ROS were also explored. For this, dimethyl sulfoxide (DMSO) and p-benzoquinone (BQ), which are the scavengers for $OH^{\bullet}$ and $O_2^{\bullet-}$, respectively, were selected to identify the types of ROS. Previously reports implied that the second-order rate constant of the reaction between DMSO and $OH^{\bullet}$ ($k = 5.4 \times 10^9$ M^{-1} s^{-1}) was greater than that of luminol with $OH^{\bullet}$ (4.8×10^9 M^{-1} s^{-1}).[37-38] However, the influence of DMSO on the ECL intensity was negligible, even when the concentration of DMSO was up to 10 mM (Figure S3a), suggesting $OH^{\bullet}$ was not apparently produced in ORR. Interestingly, despite the reaction rate constant between BQ and $O_2^{\bullet-}$ ($k = 9.6 \times 10^8$ M^{-1} s^{-1}) is approximate four times faster than luminol with $O_2^{\bullet-}$ ($k = 2.3 \times 10^8$ M^{-1} s^{-1}), a clear inhibition of ECL by BQ was found, even under a low concentration of 0.2 mM (Figure S3b).[39-40] The decreased activity by raising the concentration of BQ in the reaction further demonstrated $O_2^{\bullet-}$ was generated during ORR, consistent to the modified Damjanovic model, and consequently participated the ECL emitting.

Next, we explored whether ROS could trigger chemiluminescence of luminol. For this purpose, H_2O_2, $OH^{\bullet}$, and $O_2^{\bullet-}$, were individually produced (Figure S4) and reacted with luminol. As shown in Figure 2b, the maximum emission at ca. 440 nm was observed in all cases, which was almost identical to the fluorescence spectrum of luminol. The slight red shift of the chemiluminescence spectrum compared to the photoexcited spectrum was noticed, attributing to an inner filter effect of luminol.[41] Due to electrochemical oxidation, when applied an oxidation potential, e.g., at 0.3 V, the chemiluminescence of luminol was significantly boosted (Figure S5). Thus, the chemiluminescence of luminol could be triggered by ROS or/and electrochemical oxidation.

To check the stability of ROS, the duration of the ECL triggered by ROS was studied. As shown in Figure 2c, the ECL decay had an exponential shape, which indicated that the concentration of ROS near the surface of electrode was exponentially decreasing in time, and practically, the concentration of ROS can be analyzed up to 10 s. As discussed in the following text and SI (Figure S6), a short duration of time, i.e., 5 s, was used for ECL intensity collection in ORR kinetics evaluation.

The last but not less important requirement is that the introduction of ECL probe should not bring significant influence on ORR. In general, introducing excessive extraneous substance may influence the ORR kinetics[42-43]. Nevertheless, the polarization curves on RRDE, e.g., by Pt/C, under hydrodynamic conditions showed that such impact was weak (< 1%) in the presence of luminol up to 0.1 mM, especially in the kinetics-controlled region (Figure 2d). Such phenomenon could be explained by the fact that an alkaline environment would weaken the adsorption strength of luminol on catalyst surfaces, thanks to an electric repulsion effect.[44-45] The slightly reduced limiting current of mixed solution might be caused by a slower O_2 mass transport rate than the purely alkaline solution.[46] In this sense, rational selecting ECL luminophores in a proper concentration, the potential interference to the ORR kinetics can be minimized.

Since all the requirements for the combined ORR and ECL reactions were satisfied in principle, the ECL intensities by different electrocatalysts after ORR were collected using a double-potential step chronoamperometry (E_1, E_2), in which, E_1 was used to drive ORR, and when E_2 at 0.3 V was applied, ORR was terminated and ECL was simultaneously triggered. As a proof of concept, the ECL intensity of two typical precious group metal (PGM)-free electrocatalysts, i.e., N-C and Fe-N-C-0.5, were firstly measured as the function of E_{Red}. It was found that the ECL intensity of Fe-N-C-0.5 was low and almost kept constant at all measured E_{Red} (Figure 3a); while that of N-C became much higher and varied significantly at different potential (Figure 3b). In order to better show the effects of ROS on the ECL profiles, the changes of ECL (Δ ECL) were plotted against different potentials (Figure 3c). The ECL intensity, where E_1 was 0 V and E_2 was 0.3 V, was set as the benchmark and named it as ECL_0. Since the ECL intensity was proportional to the concentration of ROS (Eq. 3-9), it indicated that the ORR of Fe-N-C-0.5 at each E_1 only produced a small amount of ROS. In contrast, stronger ECL emissions from N-C were obtained, e.g., by a factor up to 100 times at E_1 of -0.3 V (Figure 3c), manifesting generation of abundant ROS during ORR.

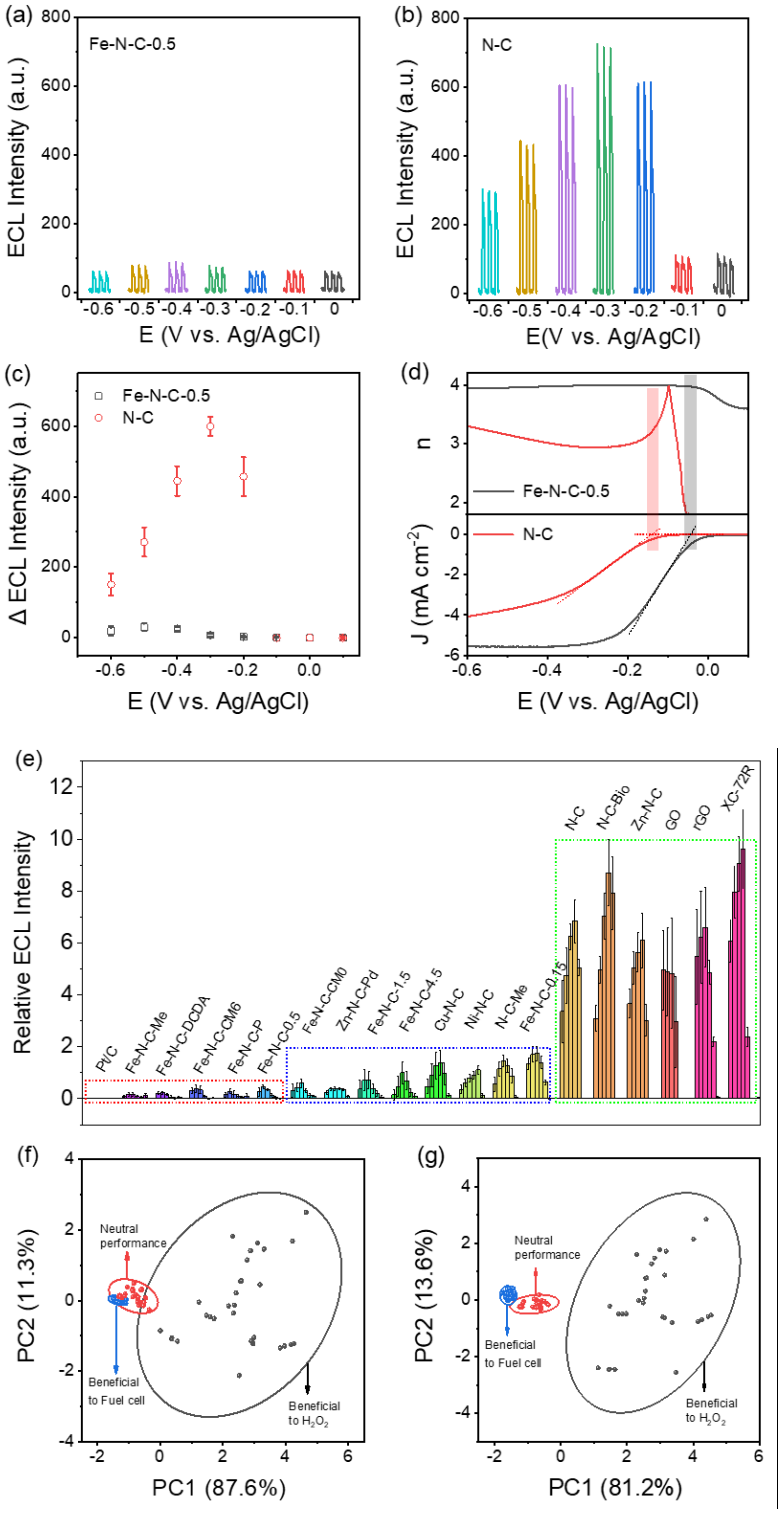

Figure 3. Qualitative evaluation of Electrocatalytic ORR activity using EC-ECL. Raw ECL signal of (a) Fe-N-C-0.5-luminol system and (b) N-C-luminol system by double-potential step chronoamperometry (E_{Red}, E_{Ox}). (c) The changed ECL intensity of Fe-N-C-0.5-luminol system and N-C -luminol system at varied E_{Red}. (d) Potential dependent variation of n (top) and LSV (bottom) of electrocatalysts. (e) Calibrated relative ECL intensity ($\Delta ECL/ECL_0$) of different electrocatalysts

at varied E_{Red}. (f) PCA scatterplot from relative ECL intensity of different electrocatalysts. (g) PCA scatterplot from relative ECL intensity and reduction peak potential (E_{pc}) of different electrocatalysts. Solid cycle lines correspond to the 95% confidence interval of the spread for each cluster.

As a control, the hydrodynamic linear sweep voltammetry (LSV) curves were recorded by RRDE at rotation rate of 1600 rpm in an O_2-saturated 0.1 M KOH solution with 10 mV s^{-1} sweep rate and negative scan polarity. The associated electron transfer number (n) for the two selected electrocatalysts was shown in Figure 3d. The n value of Fe-N-C-0.5 was close to 4, particularly at the potentials negative than the onset potential of -0.05 V was reached, indicating a $4e^-$ pathway; while that of N-C was ca. 3, suggesting a mixed $2e^-/4e^-$ pathway. Interestingly, considering the description of ROS in the modified Damjanovic model in Figure 1a, the trends of ECL intensity were practically consistent with the RRDE result. Nonetheless, the RRDE method need to manually select reliable ORR data by use of Eq. S4, 5, as an abnormal extreme of n value was generated at potentials when ORR started, while the ECL approach not. Other eighteen electrocatalysts comprising of typical doped carbon and noble metals/alloys were also examined, which showed the similar results (Figure S9b-28b). In this sense, the inspection of ROS-intermediates enabled by ultrasensitive ECL showed potentials in disclosure of kinetic information of ORR with generality in the whole potential window.

Considering that the different catalytic ability of electrocatalysts for luminol leads to different ECL_0, the relative ECL intensity calibrated as $\Delta ECL/ECL_0$ to demonstrate the intrinsic capability of the electrocatalysts in generating ROS in ORR. As shown in Figure 3e, the calibrated ECL intensity could approximately divided into three groups. Using the calibrated ECL intensity and n values of the well-known N-C ($3e^-$) and Fe-N-C-0.5 ($4e^-$) as the reference, the n of electrocatalysts in the same group was roughly estimated to be similar. For the other electrocatalysts, their n values were supposed to position between them. These speculations were consistent to the RRDE measurements (Figure S9-28). As the calibrated ECL intensity were convenient to be obtained and

analyzed, making it promising to rapidly guide electrocatalysts for fuel cell or H_2O_2 production as a preliminary evaluation tool according to the electron transfer number.

To better associate the n value of electrocatalysts to the sophisticated ECL, the principal component analysis (PCA) that can maximize variance was further applied.[47-48] By reducing the dimensionality, the data set was displayed in a score plots with a coordinate system that best discriminates it. In the first attempt, the date set, including the calibrated ECL intensity obtained from various E_{Red} with five repetitive trials for each electrocatalysts, were used for the PCA processes. In the scatter graph (Figure 3f), a circle can be marked, representing an exclusive zone for a specific type of electrocatalyst, namely, beneficial to fuel cell, H_2O_2 production, or other specific applications. Nonetheless, some minor overlap of the circled zone was noted, indicating the insufficient discrimination mostly because of the deficiency of uncorrelated variables. In fact, the cathodic peak potential (E_{pc}) was simultaneously obtained by EC-ECL measurements, and was also an important kinetic parameter for ORR. Further introducing E_{pc} into the data set for PCA, all the tested can be mostly discriminated with the 95% confidence ellipses (Figure 3g). Therefore, thanks to ROS generation in ORR by different electrocatalysts, the comprehensive PCA well discriminated the associated ECL and classified electrocatalysts according to different electron transfer numbers.

Beyond qualitative classification of electrocatalysts according to requirements for different applications via average results by PCA, the quantitative determination of ORR kinetics, particularly at different potential is essential for full evaluation of electrocatalyst performances and understanding the degradation mechanism. Because the ECL signal is associated with ROS and the concentration of ROS is a kind of embodiment for ORR kinetics, it suggested that the ORR kinetics can be disclosed by finite element analysis (FEA) of the ECL decay curve. Figure 4a shows the ECL intensity as a function of time for different ORR electrocatalysts, which exhibited variable maxima and decay profile, implying distinctive ORR kinetics. For this, the classic Damjanovic model to preliminarily adopt to describe each electrochemical and chemical reaction involved in ORR (Figure 1a). The mechanism of the afterward ECL

of luminol (LH^-, the conjugated base in alkaline solution) was outlined in Eq. 1-8:

$$HO_2^- + OH^- - e^- \longrightarrow O_2^{\bullet-} + H_2O \quad (1)$$

$$LH^- + OH^- - e^- \xrightarrow{k_{app\text{-}LH^-}} L^{\bullet-} + H_2O \quad (2)$$

$$L^{\bullet-} + O_2 \xrightarrow{k1} O_2^{\bullet-} + L \quad (3)$$

$$L^{\bullet-} + O_2^{\bullet-} + H_2O \xrightarrow{k2} L^-O_2H + OH^- \quad (4)$$

$$L^{\bullet-} + L^{\bullet-} + H_2O \xrightarrow{k3} L + LH^- + OH^- \quad (5)$$

$$L + HO_2^- \xrightarrow{k4} L^-O_2H \quad (6)$$

$$L^-O_2H \xrightarrow{k5} Ap^* + N_2 \quad (7)$$

$$Ap^* \xrightarrow{k6} Ap + h\nu \quad (8)$$

Since the concentration of LH^- was a constant in the experiment, the amounts of photon-emitting species (Ap*) rendered a positive correlation to that of ROS. The ECL intensity was dynamically proportional to the concentration of Ap* at any given time depending on the relative rates of formation and consumption. The intensity of ECL was simulated by FEA by using the transient concentration of Ap* as follows []:

$$I_{ECL}(t) = \phi_{ECL} k_{app\text{-}LH^-} \int_V [Ap^*](t)dV \quad (9)$$

where ϕ_{ECL} is the overall quantum yield, $k_{app\text{-}LH^-}$ is the apparent reaction rate constant, t is the time, and V is the volume of Ap* solution.

For simplicity, four hypothesis and approximation were employed in establishing the rate equation. Firstly, for each electrocatalyst, the ORR reaction occurred via a mixed and competitive $2e^-$ and $4e^-$ pathway. In the $2e^-$ process, O_2 was reduced to H_2O_2 via $O_2^{\bullet-}$ intermediates, and the further reduction into OH^- or H_2O was omitted due to the slow reaction rate constant. In the $4e^-$ process, O_2 was supposed to reduce to H_2O directly. As such, a rate constant ratio of the $4e^-$ to the $2e^-$ pathway (the apparent reaction rate constant, k_{Red}^{2e}), m, can be used to describe the level of participation for each pathway. Secondly, the reduction reaction rate of $O_2^{\bullet-}$ to H_2O_2, the rate determining step, was assumed to be 10 times that of O_2 to $O_2^{\bullet-}$.[24, 49] Thirdly, ROS production occurred only

in the diffusion layer by $2e^-$ pathway, while not in the 4e- pathway, and the concertation in bulk solution was set as zero. Lastly, the detailed adsorption/desorption of O_2 and ROS on the electrocatalysts was not considered.

To extract k_{Red}^{2e} from the experimental ECL decay curve, a series of simulated ECL were generated by the time dependent mass balance equation (Eq. 10) and flux expression (Eq. 11, 12):

$$\frac{\partial c_i}{\partial t} + \nabla \cdot (-D_i \nabla c_i) + \mathrm{u} \cdot \nabla c_i = R_i \quad (10)$$

$$-N_{0,\mathrm{O}} = k_{\mathrm{Red}}[\mathrm{O}] - k_{\mathrm{Ox}}[\mathrm{R}] \quad (11)$$

$$-N_{0,\mathrm{R}} = k_{\mathrm{Ox}}[\mathrm{O}] - k_{\mathrm{Red}}[\mathrm{R}] \quad (12)$$

where R_i is the reaction rate of species i, $-D_i \nabla c_i$ is the diffusion term, and $\mathrm{u} \cdot \nabla c_i$ is the convection term, c_i and D_i are the local concentration and diffusion coefficient of redox species. $N_{0,\mathrm{O}}$ and $N_{0,\mathrm{R}}$ are the user defined flux expression relevant to the species O and species R, respectively. k_{Red} and k_{Ox} is the apparent reaction rate constant of the reduction of species O to species R and the oxidation of species R to species O, respectively. [O] is the concentration of O_2 and [R] is the concentration of $O_2^{\bullet-}$ in the reduction reaction of O_2 to $O_2^{\bullet-}$. [O] is the concentration of $O_2^{\bullet-}$ and [R] is the concentration of H_2O_2 in the reduction reaction of $O_2^{\bullet-}$ to H_2O_2. In this work, the flux expression was dependent on the applied potential and the concentration of redox species at the electrode surface (see the Supporting Information for details). For example, as shown in Figure 4b, the best fit for Zn-N-C at -0.6 V was determined from the highest coefficient of determination (R^2) value, corresponding to k_{Red}^{2e} value of 6.67×10^{-3} cm s^{-1}. Along this line, k_{Red}^{2e} of other electrocatalysts were similarly obtained (Figure S31-37), following the order of XC-72R > rGO > Zn-N-C > N-C > Fe-N-C-CM6 > Fe-N-C-DCDA > Fe-N-C-Me (Figure 4c). Evidently, among them, XC-72R was more suitable for H_2O_2 production; in contrast, k_{Red}^{2e} of Fe-N-C-Me was nearly two orders of magnitude lower than that of XC-72R, manifesting that Fe-N-C-Me was more inclined to a $4e^-$ reduction pathway.

Despite the success in comparing the simulated k_{Red}^{2e} of different catalysts, the k_{Red}^{2e} at different potential did not always follow the trend of getting larger with the more negative potential.[50] To address this deviation, rather than simply using the relative magnitude between k_{Ox} at 0.3 V and k_{Red} at -0.3 to -0.6 V to get the suitable k_{Red}^{2e}, the Butler–Volmer (BV) formulation that quantitatively describes the relationship between the rate constant and applied potential was further used in Eq. 13, which is shown as follows:

$$k_{\mathrm{Red}}^{\mathrm{B\text{-}V,2e}} = k^{0,2e} e^{-\alpha \frac{F}{RT}(E_{\mathrm{Red}} - E^{0,2e})} \quad (13)$$

where $k_{\mathrm{Red}}^{\mathrm{B\text{-}V,2e}}$ is the rate constant for the reduction reaction derived from the BV model, $k^{0,2e}$ is the standard rate constant, E_{Red} is the applied potential, $E^{0,2e}$ is the standard redox potential, α is the transfer coefficient, F is Faraday's constant, R is the ideal gas constant and T is the temperature.

Taking Zn-N-C of $2e^-$ pathway (Figure 4d, Figure S38) and Fe-N-C-Me of $4e^-$ pathway (Figure 4g, Figure S39) for example, the simulated ECL intensity approached the experimental one, resulting in ($E^{0,2e}$, $k^{0,2e}$) of (-0.38 V, 6.75×10^{-4} cm s^{-1}) and (-0.27 V, 2.75×10^{-5} cm s^{-1}), respectively. Notably, to eliminate the potential differences in drive ECL of luminol by different electrocatalysts, the $k_{\mathrm{app\text{-}LH}}$- of each electrocatalyst was corrected using the ECL intensity of themselves at E_{Red} of 0 V and E_{ox} of 0.3 V during Tr-ECL measurements (see the Supporting Information for details). Along this line, the variation of ROS concentration at different applied potentials was further simulated. Considering the accumulation time for ROS in ORR, a duration of 5 s was selected as the initial value for the simulation. For Zn-N-C, the simulated concentration of $O_2^{\bullet-}$ was smaller both at low or high overpotentials, while that at the middle ground position was higher (Figure 4e). Conversely, simulated concentration of H_2O_2 kept increasing with the increase of overpotentials (Figure 4f). Interestingly, the ROS concentration at different potentials for Fe-N-C-Me was much lower than that of Zn-N-C, but the trend was similar (Figure 4g, h). Considering that in alkaline electrolytes $O_2^{\bullet-}$ would damage the electrocatalyst active site and accordingly shorten the electrocatalyst lifetime, it was assumed that the choice of a smaller overpotential would

be preferred to ORR electrocatalyst of 4e- reduction pathway for fuel cells, owing to the simultaneously lower concentration of $O_2^{\bullet-}$ and higher output voltage. In contrast, the selection of a larger overpotential would be beneficial to ORR electrocatalyst of 2e- reduction pathway for H_2O_2 manufacture, because of the simultaneously high yield of H_2O_2 and low concentration of $O_2^{\bullet-}$. Such information was critical to guide the specific application of ORR electrocatalysts with both maximized performance and stability.

The $E^{0,2e}$and $k^{0,2e}$ values are difficult to derive due to the irreversible voltammograms for O_2 reduction to $O_2^{\bullet-}$. Several works had used to get k^0 values by cyclic voltammetry and SECM methods. For example, a study of ORR at a methylphenyl-modified carbon electrode in 1 M KOH, $k^0 = 2.6\times10^{-4}$ cm s^{-1} was reported.[51] Bard, *et al*. observed $k^0 = 3\times10^{-3}$ cm s^{-1} from a simple 1e transfer of ORR in 10 M NaOH solution by SECM.[52] Compton, *et al*. observed $k^0 = 3\times10^{-1}$ cm s^{-1} on a gold macroelectrode and $k^0 = 2.1\times10^{-1}$ cm s^{-1} at an electrodeposited gold nanoparticle-modified glassy carbon electrode (GCE) in 0.5 M sulfuric acid (H_2SO_4).[53] Also, they reported $k^0 \sim 10$ cm s^{-1} at a platinum nanoparticles-modified GCE in 0.5 M H_2SO_4.[49] In addition, Hasnat, *et al*. suggested that a k^0 of 5.48×10^{-9} cm s^{-1} was got at +0.05 V vs. Ag/AgCl (sat. KCl) at gold nanoparticle-modified GCE in 0.1 M H_2SO_4.[54] It can be seen that the k^0 value has a large span in the previous work. Considering that our work examines the complex four-electron reaction of ORR, and the fact that the used electrocatalysts and medium are also different from that used in previous work, the occurrence of $k^{0,2e}$ with different values is well documented. In addition, according to Eq. 9-13, as related to the concentration of AP* and the associated ECL intensity, the absolute value of $k^{0,2e}$ by the proposed Tr-ECL method contained photonic information of ECL probes, therefore, their relative values are practical rather than the absolute ones.

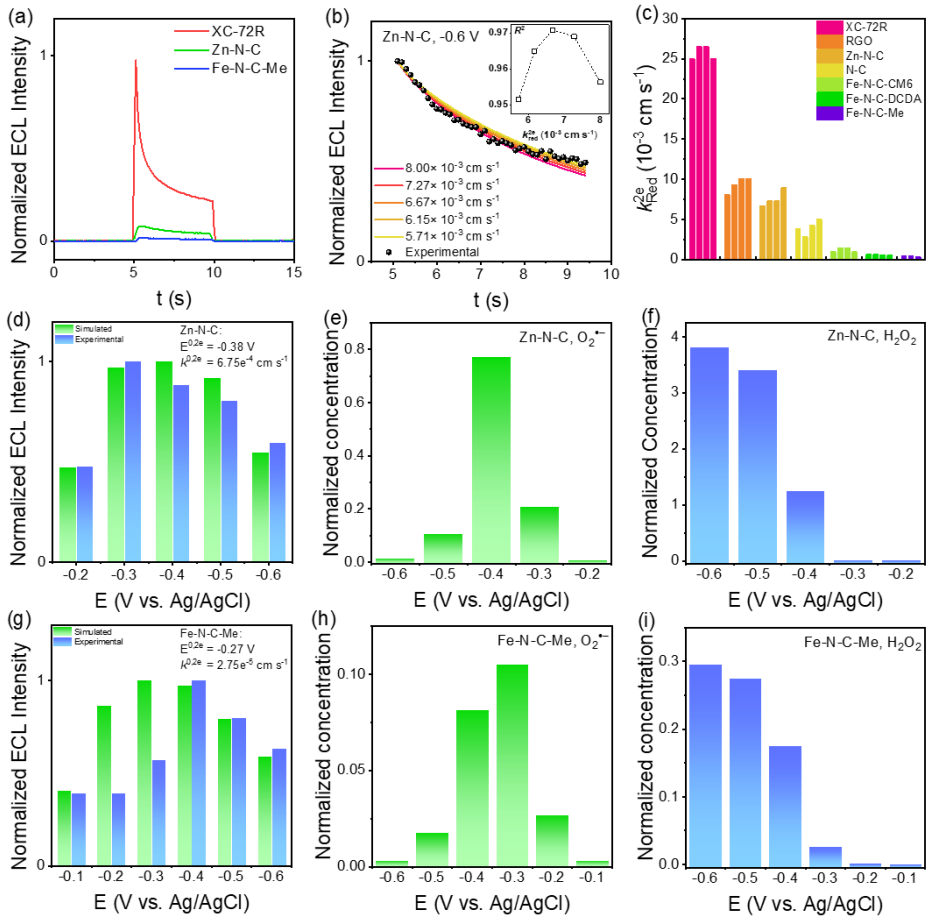

Figure 4. Determination of ORR kinetics via the combination of experimental measurement and simulation. (a) ECL intensity as a function of time for XC-72R, Zn-N-C, Fe-N-C-Me at E_{Red} = -0.6 V and E_{Ox} = 0.3 V. (b) Decay curves of experimental ECL data (Zn-N-C, black solid line) and simulated ECL data (dashed line) at E_{Red} of -0.6 V and E_{Ox} of 0.3 V. Inset: the R^2 values from comparisons of experimental ECL to simulated curves. (c) Comparison of extracted k_{Red}^{2e} of different electrocatalysts. Simulated (green) and experimental (blue) ECL intensity by (d) Zn-N-C and (g) Fe-N-C-Me at ($E^{0,2e}$, $k^{0,2e}$) of (-0.38 V, 6.75×10^{-4} cm s^{-1}) and (-0.27 V, 2.75×10^{-5} cm s^{-1}), respectively, and the corresponding concentration of ROS of (e, f) Zn-N-C and (h, i) Fe-N-C-Me at different potentials.

Conclusion

In summary, we devised a simple yet powerful strategy for kinetic evaluation of ORR electrocatalyst by ultrasensitive ECL in a conventional electrochemical three-electrode cell configuration (Tr-ECL). The strategy used the trace-amount of ROS intermediates that were generated during ORR process to establish the reaction rate equation. It

intrinsically circumvented the challenge of maintaining high mass transfer of O_2 in electrolytes during ORR in previous mainstream methods, such as RDE/RRDE and FET, meanwhile demonstrating great convenience compared to MEA and SECM approaches. The ECL intensity and basic cathodic wave of different electrocatalysts in the stationary condition can be fast screened by PCA, making electrocatalysts be divided into groups according to different electron transfer numbers. Further by FEA of the ECL decay curves, the apparent kinetic constants of electrocatalysts in ORR could be quantitatively fitted. Moreover, the FEA exclusively revealed the information of the distribution of ROS in the diffusion layer at different potentials, unavailable by the traditional kinetic evaluation methods, which would greatly facilitate the rational development of electrocatalysts with improved stability. Further work is underway focusing on the kinetic evaluation of other electrochemical energy reactions, such as hydrogen evolution reaction and oxygen evolution reaction.

Referrence

1. Ahn, C.-Y.; Park, J. E.; Kim, S.; Kim, O.-H.; Hwang, W.; Her, M.; Kang, S. Y.; Park, S.; Kwon, O. J.; Park, H. S.; Cho, Y.-H.; Sung, Y.-E., Differences in the Electrochemical Performance of Pt-Based Catalysts Used for Polymer Electrolyte Membrane Fuel Cells in Liquid Half- and Full-Cells. *Chemical Reviews* 2021, *121* (24), 15075-15140.
2. He, Y.; Liu, S.; Priest, C.; Shi, Q.; Wu, G., Atomically dispersed metal–nitrogen–carbon catalysts for fuel cells: advances in catalyst design, electrode performance, and durability improvement. *Chemical Society Reviews* 2020, *49* (11), 3484-3524.
3. Debe, M. K., Electrocatalyst approaches and challenges for automotive fuel cells. *Nature* 2012, *486* (7401), 43-51.
4. Kodama, K.; Nagai, T.; Kuwaki, A.; Jinnouchi, R.; Morimoto, Y., Challenges in applying highly active Pt-based nanostructured catalysts for oxygen reduction reactions to fuel cell vehicles. *Nature Nanotechnology* 2021, *16* (2), 140-147.
5. Yu, P.; Wang, L.; Sun, F.; Xie, Y.; Liu, X.; Ma, J.; Wang, X.; Tian, C.; Li, J.; Fu, H., Co Nanoislands Rooted on Co–N–C Nanosheets as Efficient Oxygen Electrocatalyst for Zn–Air Batteries. *Advanced Materials* 2019.
6. Jiang, Y.; Deng, Y.-P.; Liang, R.; Fu, J.; Gao, R.; Luo, D.; Bai, Z.; Hu, Y.; Yu, A.; Chen, Z., d-Orbital steered active sites through ligand editing on heterometal imidazole frameworks for rechargeable zinc-air battery. *Nature Communications* 2020, *11* (1).
7. Nørskov, J. K.; Rossmeisl, J.; Logadottir, A.; Lindqvist, L.; Kitchin, J. R.; Bligaard, T.; Jónsson, H., Origin of the Overpotential for Oxygen Reduction at a Fuel-Cell Cathode. *The Journal of Physical Chemistry B* 2004, *108* (46), 17886-17892.
8. Liu, Z.; Zhao, Z.; Peng, B.; Duan, X.; Huang, Y., Beyond Extended Surfaces: Understanding the Oxygen Reduction Reaction on Nanocatalysts. *Journal of the American Chemical Society* 2020, *142* (42), 17812-17827.
9. Jiao, L.; Li, J.; Richard, L. L.; Sun, Q.; Stracensky, T.; Liu, E.; Sougrati, M. T.; Zhao, Z.; Yang, F.; Zhong, S.; Xu, H.; Mukerjee, S.; Huang, Y.; Cullen, D. A.; Park, J. H.; Ferrandon, M.; Myers, D. J.; Jaouen, F.; Jia, Q., Chemical vapour deposition of Fe–N–C oxygen reduction catalysts with full utilization of dense Fe–N4 sites. *Nature Materials* 2021, *20* (10), 1385-1391.
10. Seh, Z. W.; Kibsgaard, J.; Dickens, C. F.; Chorkendorff, I.; Nørskov, J. K.; Jaramillo, T. F., Combining theory and experiment in electrocatalysis: Insights into materials design. *Science* 2017, *355* (6321).
11. Zaman, S.; Huang, L.; Douka, A. I.; Yang, H.; You, B.; Xia, B. Y., Oxygen Reduction Electrocatalysts toward Practical Fuel Cells: Progress and Perspectives. *Angewandte Chemie International Edition* 2021, *60* (33), 17832-17852.
12. Martens, S.; Asen, L.; Ercolano, G.; Dionigi, F.; Zalitis, C.; Hawkins, A.; Martinez Bonastre, A.; Seidl, L.; Knoll, A. C.; Sharman, J.; Strasser, P.; Jones, D.; Schneider, O., A comparison of rotating disc electrode, floating electrode technique and membrane electrode assembly measurements for catalyst testing. *Journal of Power Sources* 2018, *392*, 274-284.
13. Zhou, R.; Zheng, Y.; Jaroniec, M.; Qiao, S.-Z., Determination of the Electron Transfer Number for the Oxygen Reduction Reaction: From Theory to Experiment. *ACS Catalysis* 2016, *6* (7), 4720-4728.
14. Dong, K.; Liang, J.; Wang, Y.; Xu, Z.; Liu, Q.; Luo, Y.; Li, T.; Li, L.; Shi, X.; Asiri, A. M.; Li, Q.; Ma, D.; Sun, X., Honeycomb Carbon Nanofibers: A Superhydrophilic O

2

-Entrapping Electrocatalyst Enables Ultrahigh Mass Activity for the Two-Electron Oxygen Reduction Reaction. *Angewandte Chemie International Edition* 2021, *60* (19), 10583-10587.
15. Yang, Z.; Yang, H.; Shang, L.; Zhang, T., Ordered PtFeIr Intermetallic Nanowires Prepared through a Silica-Protection Strategy for the Oxygen Reduction Reaction. *Angewandte Chemie International Edition* 2021, *61* (8).
16. Fan, J.; Chen, M.; Zhao, Z.; Zhang, Z.; Ye, S.; Xu, S.; Wang, H.; Li, H., Bridging the gap between highly active oxygen reduction reaction catalysts and effective catalyst layers for proton exchange membrane fuel cells. *Nature Energy* 2021, *6* (5), 475-486.
17. Zalitis, C. M.; Kramer, D.; Kucernak, A. R., Electrocatalytic performance of fuel cell reactions at low catalyst loading and high mass transport. *Physical Chemistry Chemical Physics* 2013, *15* (12).
18. Jackson, C.; Lin, X.; Levecque, P. B. J.; Kucernak, A. R. J., Toward Understanding the Utilization of Oxygen Reduction Electrocatalysts under High Mass Transport Conditions and High Overpotentials. *ACS Catalysis* 2021, *12* (1), 200-211.
19. Bard, A. J.; Fan, F.-R. F.; Pierce, D. T.; Unwin, P. R.; Wipf, D. O.; Zhou, F., Chemical Imaging of Surfaces with the Scanning Electrochemical Microscope. *Science* 1991, *254* (5028), 68-74.
20. Amemiya, S.; Bard, A. J.; Fan, F.-R. F.; Mirkin, M. V.; Unwin, P. R., Scanning Electrochemical Microscopy. *Annual Review of Analytical Chemistry* 2008, *1* (1), 95-131.
21. Preet, A.; Lin, T.-E., A Review: Scanning Electrochemical Microscopy (SECM) for Visualizing the Real-Time Local Catalytic Activity. *Catalysts* 2021, *11* (5).
22. Zhou, M.; Yu, Y.; Hu, K.; Mirkin, M. V., Nanoelectrochemical Approach To Detecting Short-Lived Intermediates of Electrocatalytic Oxygen Reduction. *Journal of the American Chemical Society* 2015, *137* (20), 6517-6523.
23. Dong, J.-C.; Zhang, X.-G.; Briega-Martos, V.; Jin, X.; Yang, J.; Chen, S.; Yang, Z.-L.; Wu, D.-Y.; Feliu, J. M.; Williams, C. T.; Tian, Z.-Q.; Li, J.-F., In situ Raman spectroscopic evidence for oxygen reduction reaction intermediates at platinum single-crystal surfaces. *Nature Energy* 2018, *4* (1), 60-67.
24. Gómez-Marín, A. M.; Feliu, J. M.; Ticianelli, E., Oxygen Reduction on Platinum Surfaces in Acid Media: Experimental Evidence of a CECE/DISP Initial Reaction Path. *ACS Catalysis* 2019, *9* (3), 2238-2251.
25. Chen, M.-M.; Xu, C.-H.; Zhao, W.; Chen, H.-Y.; Xu, J.-J., Super-Resolution Electrogenerated Chemiluminescence Microscopy for Single-Nanocatalyst Imaging. *Journal of the American Chemical Society* 2021, *143* (44), 18511-18518.
26. Maar, R. R.; Zhang, R.; Stephens, D. G.; Ding, Z.; Gilroy, J. B., Near-Infrared Photoluminescence and Electrochemiluminescence from a Remarkably Simple Boron Difluoride Formazanate Dye. *Angewandte Chemie International Edition* 2019, *58* (4), 1052-1056.
27. Ma, X.; Gao, W.; Du, F.; Yuan, F.; Yu, J.; Guan, Y.; Sojic, N.; Xu, G., Rational Design of Electrochemiluminescent Devices. *Accounts of Chemical Research* 2021, *54* (14), 2936-2945.
28. Dong, J.; Lu, Y.; Xu, Y.; Chen, F.; Yang, J.; Chen, Y.; Feng, J., Direct imaging of single-molecule electrochemical reactions in solution. *Nature* 2021, *596* (7871), 244-249.
29. Lv, Y.; Chen, S.; Shen, Y.; Ji, J.; Zhou, Q.; Liu, S.; Zhang, Y., Competitive Multiple-Mechanism-Driven Electrochemiluminescent Detection of 8-Hydroxy-2′-deoxyguanosine. *Journal of the American Chemical Society* 2018, *140* (8), 2801-2804.
30. Gu, W.; Wang, H.; Jiao, L.; Wu, Y.; Chen, Y.; Hu, L.; Gong, J.; Du, D.; Zhu, C., Single-Atom Iron Boosts Electrochemiluminescence. *Angewandte Chemie International Edition* 2020, *59* (9), 3534-3538.
31. Li, L.; Chen, Y.; Zhu, J.-J., Recent Advances in Electrochemiluminescence Analysis. *Analytical*

Chemistry 2016, *89* (1), 358-371.
32. Miao, W., Electrogenerated Chemiluminescence and Its Biorelated Applications. *Chemical Reviews* 2008, *108* (7), 2506-2553.
33. Zhao, W.; Chen, H.-Y.; Xu, J.-J., Electrogenerated chemiluminescence detection of single entities. *Chemical Science* 2021, *12* (16), 5720-5736.
34. Hsueh, K. L.; Chin, D. T.; Srinivasan, S., Electrode kinetics of oxygen reduction. *Journal of Electroanalytical Chemistry and Interfacial Electrochemistry* 1983, *153* (1-2), 79-95.
35. Wu, F.; Pan, C.; He, C.-T.; Han, Y.; Ma, W.; Wei, H.; Ji, W.; Chen, W.; Mao, J.; Yu, P.; Wang, D.; Mao, L.; Li, Y., Single-Atom Co–N4 Electrocatalyst Enabling Four-Electron Oxygen Reduction with Enhanced Hydrogen Peroxide Tolerance for Selective Sensing. *Journal of the American Chemical Society* 2020, *142* (39), 16861-16867.
36. Wang, J.; Wang, K.; Wang, F.-B.; Xia, X.-H., Bioinspired copper catalyst effective for both reduction and evolution of oxygen. *Nature Communications* 2014, *5* (1).
37. Bardouki, H.; da Rosa, M. B.; Mihalopoulos, N.; Palm, W. U.; Zetzsch, C., Kinetics and mechanism of the oxidation of dimethylsulfoxide (DMSO) and methanesulfinate (MSI−) by OH radicals in aqueous medium. *Atmospheric Environment* 2002, *36* (29), 4627-4634.
38. Schiller, J.; Arnhold, J.; Schwinn, J.; Sprinz, H.; Brede, O.; Arnold, K., Differences in the reactivity of phthalic hydrazide and luminol with hydroxyl radicals. *Free Radical Research* 2009, *30* (1), 45-57.
39. Bandara, J.; Kiwi, J., Fast kinetic spectroscopy, decoloration and production of H2O2 induced by visible light in oxygenated solutions of the azo dye Orange II. *New Journal of Chemistry* 1999, *23* (7), 717-724.
40. Koizumi, Y.; Nosaka, Y., Kinetics Simulation of Luminol Chemiluminescence Based on Quantitative Analysis of Photons Generated in Electrochemical Oxidation. *The Journal of Physical Chemistry A* 2013, *117* (33), 7705-7711.
41. Sartin, M. M.; Camerel, F.; Ziessel, R.; Bard, A. J., Electrogenerated Chemiluminescence of B8amide: A BODIPY-Based Molecule with Asymmetric ECL Transients. *The Journal of Physical Chemistry C* 2008, *112* (29), 10833-10841.
42. Qu, L.; Liu, Y.; Baek, J.-B.; Dai, L., Nitrogen-Doped Graphene as Efficient Metal-Free Electrocatalyst for Oxygen Reduction in Fuel Cells. *ACS Nano* 2010, *4* (3), 1321-1326.
43. He, D.; Zhong, L.; Gan, S.; Xie, J.; Wang, W.; Liu, Z.; Guo, W.; Yang, X.; Niu, L., Hydrogen peroxide electrosynthesis via regulating the oxygen reduction reaction pathway on Pt noble metal with ion poisoning. *Electrochimica Acta* 2021, *371*.
44. Zhu, S.; Hu, X.; Shao, M., Impacts of anions on the oxygen reduction reaction kinetics on platinum and palladium surfaces in alkaline solutions. *Physical Chemistry Chemical Physics* 2017, *19* (11), 7631-7641.
45. Holst-Olesen, K.; Reda, M.; Hansen, H. A.; Vegge, T.; Arenz, M., Enhanced Oxygen Reduction Activity by Selective Anion Adsorption on Non-Precious-Metal Catalysts. *ACS Catalysis* 2018, *8* (8), 7104-7112.
46. Omura, J.; Yano, H.; Watanabe, M.; Uchida, H., Electrochemical Quartz Crystal Microbalance Analysis of the Oxygen Reduction Reaction on Pt-Based Electrodes. Part 1: Effect of Adsorbed Anions on the Oxygen Reduction Activities of Pt in HF, HClO4, and H2SO4 Solutions. *Langmuir* 2011, *27* (10), 6464-6470.
47. Stewart, S.; Ivy, M. A.; Anslyn, E. V., The use of principal component analysis and discriminant analysis in differential sensing routines. *Chem. Soc. Rev.* 2014, *43* (1), 70-84.

48. Chen, J.; Hickey, B. L.; Wang, L.; Lee, J.; Gill, A. D.; Favero, A.; Pinalli, R.; Dalcanale, E.; Hooley, R. J.; Zhong, W., Selective discrimination and classification of G-quadruplex structures with a host–guest sensing array. *Nature Chemistry* 2021, *13* (5), 488-495.
49. Gara, M.; Laborda, E.; Holdway, P.; Crossley, A.; Jones, C. J. V.; Compton, R. G., Oxygen reduction at sparse arrays of platinum nanoparticles in aqueous acid: hydrogen peroxide as a liberated two electron intermediate. *Physical Chemistry Chemical Physics* 2013, *15* (44).
50. Kato, M.; Fujibayashi, N.; Abe, D.; Matsubara, N.; Yasuda, S.; Yagi, I., Impact of Heterometallic Cooperativity of Iron and Copper Active Sites on Electrocatalytic Oxygen Reduction Kinetics. *ACS Catalysis* 2021, *11* (4), 2356-2365.
51. Yang, H.-H.; McCreery, R. L., Elucidation of the Mechanism of Dioxygen Reduction on Metal-Free Carbon Electrodes. *Journal of The Electrochemical Society* 2000, *147* (9).
52. Zhang, C.; Fan, F.-R. F.; Bard, A. J., Electrochemistry of Oxygen in Concentrated NaOH Solutions: Solubility, Diffusion Coefficients, and Superoxide Formation. *Journal of the American Chemical Society* 2008, *131* (1), 177-181.
53. Wang, Y.; Laborda, E.; Ward, K. R.; Tschulik, K.; Compton, R. G., A kinetic study of oxygen reduction reaction and characterization on electrodeposited gold nanoparticles of diameter between 17 nm and 40 nm in 0.5 M sulfuric acid. *Nanoscale* 2013, *5* (20).
54. Islam, M. T.; Hasan, M. M.; Shabik, M. F.; Islam, F.; Nagao, Y.; Hasnat, M. A., Electroless deposition of gold nanoparticles on a glassy carbon surface to attain methylene blue degradation via oxygen reduction reactions. *Electrochimica Acta* 2020, *360*.